Biochimica et Biophysica Acta, 730 (1983) 295–305
Elsevier Biomedical Press

BBA 71643

HYSTERETIC ACTIVATION OF THE Ca^{2+} PUMP REVEALED BY CALCIUM TRANSIENTS IN HUMAN RED CELLS

OLE SCHARFF, BIRTHE FODER and ULRIK SKIBSTED

Department of Clinical Physiology, Finsen Institute, Strandboulevarden 49, DK 2100 Copenhagen (Denmark)

(Received December 22nd, 1982)

Key words: Ca^{2+} pump; Ca^{2+} transient; Hysteresis; Ionophore A23187; Calmodulin; (Human erythrocyte)

The enzymatic basis for the Ca^{2+} pump in human red cells is an ATPase with hysteretic properties. The Ca^{2+}-ATPase shifts slowly between a ground state deficient in calmodulin and an active state saturated with calmodulin, and rate constants for the reversible shifts of state were recently determined at different Ca^{2+} concentrations (Scharff, O. and Foder, B. (1982) Biochim. Biophys. Acta 691, 133–143). In order to study whether the Ca^{2+} pump in intact red cells also exhibits hysteretic properties we have analysed transient increases of intracellular calcium concentrations (Ca_i), induced by the divalent cation ionophore A23187. The time-dependent changes of Ca_i were measured by use of radioactive calcium ($^{45}Ca^{2+}$) and analysed with the aid of a mathematical model, based partly on the Ca^{2+}-dependent parameters obtained from Ca^{2+}-ATPase experiments, partly on the A23187-induced Ca^{2+} fluxes determined in experiments with intact red cells. According to the model a delay in the activation of the Ca^{2+} pump is a prerequisite for the occurrence of A23187-induced calcium transients in the red cells, and we conclude that the Ca^{2+} pump in human red cells responds hysteretically. It is suggested that Ca^{2+} pumps in other types of cell also have hysteretic properties.

Introduction

Cellular calcium transients occur in different types of cell, e.g., lymphocytes [1] and platelets [2], and evoke various cellular responses such as cell motility [3], contraction in skeletal muscles [4–6] and cardiac cells [7], neuronal pace-maker activity [8], secretion from pancreatic acinar cells [9] and adrenal medullary cells [10], release of insulin from pancreatic β-cells [11], and activation of cell division [1,12].

The cytoplasmic concentration of free Ca^{2+} is regulated partly by intracellular Ca^{2+} transport mechanisms in mitochondria [13] and endoplasmic reticulum [14], partly by transport mechanisms located in the plasma membrane, i.e., Ca^{2+} channels [8,15], ion exchangers (e.g., Na^+-Ca^{2+} exchange) and Ca^{2+} pumps [16,17].

In human red cells only the plasma membrane Ca^{2+} pump seems to be present, and the enzymatic basis for this Ca^{2+} pump is an ATPase that is regulated by calcium and calmodulin (for reviews see Refs. 17–20). The Ca^{2+}-ATPase shows hysteretic properties [20]: the enzyme can occur in two different states, viz., a calmodulin-deficient and a calmodulin-saturated state, and shifts between these states have been demonstrated to be time-dependent. Recently, we have determined rate constants for the state shifts at different Ca^{2+} concentrations [21]. A similar hysteretic behaviour of the Ca^{2+} pump may contribute to the occurrence of cellular calcium transients, and this possibility can profitably be studied in the human red cell.

Transient increases of the intracellular Ca^{2+} concentration in human red cells have been ob-

Abbreviations: EGTA, ethyleneglycol bis(β-aminoethyl ether)-*N*,*N*′-tetraacetic acid.

served by treatment of the cells with the divalent cation ionophore A23187 [22–24] and propranolol [25]. The search for physiological mechanisms that by activation can increase the low Ca^{2+} permeability of the red cell membrane is still proceeding [26–28].

In the present study we have analysed A23187-induced calcium transients in intact red cells. For the analysis we have used a mathematical model based on the hysteretic properties of the Ca^{2+}-ATPase in erythrocyte membranes, and it is shown that the model can account for the A23187-induced calcium transients in the red cells.

Part of this paper was presented at the International Conference on the Ca^{2+} pump of Red Cells, in Buenos Aires, Argentina, September 13–15, 1982.

Methods

Erythrocytes were isolated from bank blood (stored 1–3 weeks), and calmodulin-deficient A-membranes and calmodulin-saturated B-membranes were prepared as earlier [29].

The red cells used for Ca^{2+} transport experiments were washed three times at 0–4°C in a standard medium containing (mM): histidine (10), imidazole (10), KCl (75), NaCl (70), $MgCl_2$ (1), pH (37°C) 7.4, and the cells were packed at 3200 $\times g$ for 10 min.

For the transport experiments, 1 vol. of packed cells were suspended in 4 vol. of standard medium, and solutions of $CaCl_2$, ^{45}Ca (10–40 mCi/mg Ca^{2+}, Amersham), EGTA, and inosine were added as detailed in Results and Discussion. The chosen concentrations of K^+ and Mg^{2+} in the standard medium were found to minimize changes in cell volume and extracellular K^+ and Mg^{2+} (cf., Ref. 22 and Results and Discussion).

Prior to the experiments, the cell suspensions were preincubated for 20–40 min at 37°C in the presence of 5–10 mM inosine (fed cells) or inosine and 7.5 mM iodoacetamide (depleted cells). After preincubation, the fed cells contained approx. 1.2 mmol ATP and 20 μmol calcium (determined by atomic absorption) per litre cells.

The Ca^{2+} transport experiments were conducted at 37°C in well stirred suspensions of fed or depleted cells. The ionophore A23187 (Calbiochem) was added from a stock solution containing 1 mg A23187 per ml of ethanol/acetone (9 : 1, v/v). For measurements of A23187-mediated Ca^{2+} influx at different extracellular Ca^{2+} concentrations the carrier-free $^{45}Ca^{2+}$ solution (approx. 20 μCi) was added to the suspension of depleted cells upon the establishment of electrochemical equilibrium with respect to ^{40}Ca, i.e., 0.5 to 3 h after the addition of ionophore A23187.

Cellular calcium was determined by a slight modification of the method of Lew et al., based on the use of ^{45}Ca [22,30]. Samples of cell suspension (200 μl) were transferred to Eppendorf centrifuge tubes, kept at 0°C, containing 850 μl of stop buffer and 400 μl of dibutylphthalate oil (density 1.042–1.045, Merck). The stop buffer contained (mM): histidine (10), imidazole (10), KCl (75), NaCl (20), $MgCl_2$ (25), EGTA (7.5), pH (20°C) 7.7. Within 2 min (see below) the tubes were centrifuged for 30 s at 13000 $\times g$. The bottom of the tube was dipped in acetone/dry ice bath, thus freezing only the cell pellet. This step (1) facilitated the aspiration of supernatant (buffer and oil) and the cleaning of tube wall with cotton swabs, and (2) haemolysed the cells before precipitation with 500 μl perchloric acid (4%). The precipitate was spun down and 420 μl of clear supernatant were transferred to 10 ml Dimilume (Packard) and counted in a Beckman liquid scintillation counter (^{14}C channel).

No significant difference in cellular radioactivity between cells centrifuged 5 s or 2 min after sampling could be detected (6 min after sampling only 2.5% of the cellular radioactivity was lost).

For determination of total or extracellular radioactivity samples of cell suspension or of supernatant from centrifuged cell suspension were precipitated with perchloric acid and counted as above.

Cellular calcium (μmol/l packed cells) was calculated from the cellular and total radioactivities and the total concentration of calcium in cell suspension. Cellular calcium, obtained from samples collected before the addition of ionophore, was regarded as a blank value, originating from the incubation medium trapped in the cell pellet. The trapped volume, consisting of incubation medium (one-sixth) and stop buffer (five-sixths), was determined to be 6%. Single flux (influx) of

Ca^{2+} was calculated from the rate of tracer equilibration, the cellular and extracellular radioactivity at equilibrium, and the concentration of calcium present in the incubation medium.

Ca^{2+}-ATPase assays, determinations of calcium, ATP, and protein were performed as previously [29,31,32]. For the calculations see Appendix.

Results and Discussion

Cellular calcium transients mediated by ionophore

Immediately after the addition of ionophore A23187 to a suspension of red cells, leading to an appropriate magnitude of Ca^{2+} influx, a transient increase of the intracellular concentration of calcium (Ca_i) could be revealed by measurements with ^{45}Ca (Fig. 1). After the peak value of Ca_i, which occurred 0.5–1 min after the ionophore A23187 addition, Ca_i decreased to a lower level that became steady, provided the cells were fuelled with inosine. Using glucose as the only energy source, we previously found that a low steady state of Ca_i could not be maintained [33].

The occurrence of a peak value of Ca_i has previously been demonstrated [22,33], and the phenomenon was suggested to be an artifact, caused by initial interactions between the ionophore and the cells before A23187-equilibration. However, as shown in Fig. 1, a cellular calcium transient could also be produced with cells equilibrated with A23187 for 10 min and then exposed to an excess of $CaCl_2$ over EGTA. 0.5 mM EGTA was present during the A23187-equilibration in order to prevent a low ionophore-mediated influx of Ca^{2+}, arising from Ca^{2+} contamination in the medium.

By repeated addition of ionophore A23187 to the same cell suspension it was possible to provoke three peak values of Ca_i, succeeded by periods in which still higher steady-state levels of Ca_i were adjusted (Fig. 2). The fourth addition of A23187 caused a dramatic increase in Ca_i (Fig. 2). Apparently, at this stage the Ca^{2+} pump was not able to compensate for the high Ca^{2+} influx, and therefore Ca_i remained high.

We suggest that the cellular calcium transients, induced by ionophore and Ca^{2+}, may reflect a genuine response of a system that regulates the concentration of ionized calcium in the red cell.

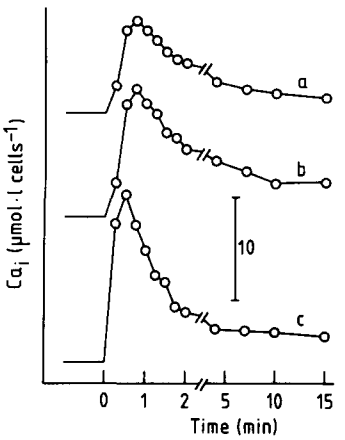

Fig. 1. Calcium transients in red cells. Cellular concentration of total calcium (Ca_i) was measured by the ^{45}Ca method (see Methods). Cellular radioactivity was measured before zero time (blank value) and was subtracted from the cellular radioactivities measured after zero time. The vertical bar refers to 10 μmol/l packed red cells. Curve *a*, fed cells in standard medium with added ^{45}Ca (approx. 20 μCi), $CaCl_2$ (100 μM), inosine (4.7 mM), and after 10 min (zero time in figure) addition of ionophore A23187 (8.8 μmol/l cells). Curve *b*, as curve *a*, except for the inclusion of 500 μM EGTA and 600 μM $CaCl_2$ in standard medium instead of 100 μM $CaCl_2$. Curve *c*, fed cells in standard medium with added A23187 (8.8 μmol/l cells), ^{45}Ca, 500 μM, EGTA, inosine, and after 10 min (zero time) addition of $CaCl_2$ solution to 600 μM.

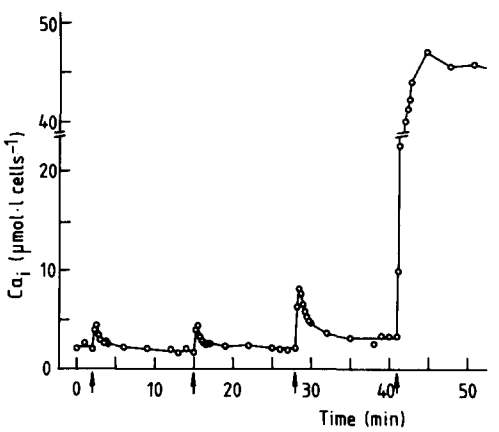

Fig. 2. Changes of cellular calcium (Ca_i) induced by successive additions of ionophore A23187. Ca_i determined as in Fig. 1, except for blank values which are included in Ca_i. The fed cells were incubated in standard medium, including approx. 20 μCi ^{45}Ca, 100 μM $CaCl_2$ and 8.9 mM inosine. The arrows indicate additions of ionophore A23187. The total ionophore A23187 concentrations after each addition were from left: 2.2, 4.4, 8.8, and 17.6 μmol/l cells.

Under the present experimental conditions the two known constituents of this system are the ionophore-mediated Ca^{2+} influx and the Ca^{2+} pump. In the last section it is shown that the cellular calcium transients can be simulated by using a mathematical model, based on the hysteretic properties of the Ca^{2+}-pump ATPase.

Before a closer analysis of the observed calcium transients we will describe the ionophore-mediated Ca^{2+} leak and the regulation of the Ca^{2+}-pump ATPase in greater detail.

Ionophore-mediated Ca^{2+} leak

Upon addition of the ionophore A23187 to a suspension of red cells, 98–99% of the added ionophore was accumulated in the cells [34] and, consequently, the Ca^{2+} permeability of the plasma membranes was increased [22,30]. The Ca^{2+} influx increased with increasing concentration of the ionophore (see Fig. 3), according to Lew and Simonsen [34] proportional to $[A]^m$, where [A] refers to A23187 concentration and $m = 1.45$. In Fig. 3, the value of m is 1.63. In another series of experiments, conducted at an extracellular Ca^{2+} concentration of approx. 300 μM at electrochemical equilibrium and various A23187 concentrations, we found $m = 1.38$. When necessary for calculations (see Fig. 8) we chose $m = 1.5$.

As expected (see Appendix, Eqn. 1), the Ca^{2+} influx was a linear function of the extracellular Ca^{2+} concentration over the range in question (Fig. 3). However, the regression lines intersect the ordinate below zero, indicating, for unknown reasons, some deviations from linearity at the lowest Ca^{2+} concentrations. To account for this non-linearity, an exponential term was included in the equation of the curves in Fig. 3.

The permeability constant, derived from the slopes of the rectilinear curve segments in Fig. 3, was only about 25% of that reported by Lew and Simonsen [34]. The main cause of this discrepancy is probably that we determined the Ca^{2+} influx in an intracellular medium containing 1 mM Mg^{2+}, while Lew and Simonsen [34] used 0.15 mM. The higher Mg^{2+} concentration resulted in a greater competition between Mg^{2+} and Ca^{2+} for the ionophore, which decreased the Ca^{2+} influx. For instance, demonstration of calcium transients in the presence of 0.15 mM Mg^{2+} (not shown) required

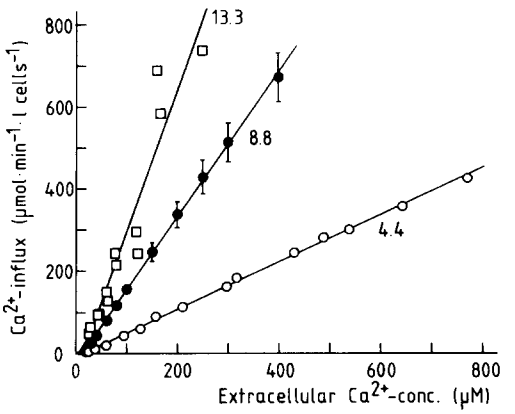

Fig. 3. Ca^{2+} influx into red cells at three different ionophore A23187 concentrations (4.4, 8.8, and 13.3 μmol/l cells) dependent on the extracellular Ca^{2+} concentration. The Ca^{2+} influx was determined in depleted cells after the establishment of electrochemical equilibrium. Single experiments (○, □) or mean ± S.E. of five experiments (●). The curves are calculated from: $y = a[Ca^{2+}] - b(1 - \exp(-[Ca^{2+}]/15))$, where a and b amount to 0.57 and 7.5 (4.4), 1.77 and 23.1 (8.8), 3.45 and 52.3 (13.3). The exponential term corrects for the non-linearity at the lowest Ca^{2+} concentrations.

lower A23187 concentrations than used in Fig. 1 in order to avoid Ca^{2+} influxes too high to be compensated for by the Ca^{2+}-pump flux.

Measurements of Mg^{2+} fluxes at different Mg^{2+} concentrations revealed that, in our experiments, 1 mM Mg^{2+} in the extracellular medium corresponded to electrochemical equilibrium, probably because we used stored bank blood in which the concentration of 2,3-diphosphoglycerate (2,3-DPG) is very low [35]. Using Flatman and Lew's data [36] and assuming zero concentration of the cellular component (2,3-DPG?) which shows large binding capacity and low affinity for Mg^{2+}, we calculated that the extracellular equilibrium concentration of Mg^{2+} would be 1 mM, in accordance with the measurements, instead of 0.15 mM which was the equilibrium concentration found in suspensions of fresh red cells [36].

Ca^{2+} dependence of A-state and B-state ATPase

Fig. 4 shows the Ca^{2+}-ATPase activities of the A state and B state in erythrocyte membranes in dependence of the concentration of free Ca^{2+}. The experimental points were fitted by an ATPase model with four activating calcium-binding sites

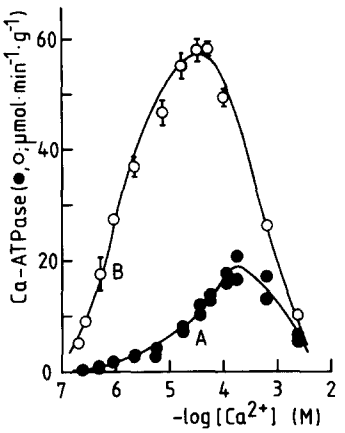

Fig. 4. Dependence of activities of Ca^{2+}-ATPase in A- and B-states on concentration of free Ca^{2+}. ATPase activity (μmol/min per g protein) of calmodulin-deficient (A) and calmodulin-saturated (B) erythrocyte membranes was assayed as previously [29]. A, single experiments. B, mean $\pm$S.E. of eight experiments. The solid curves were fitted to the experimental points by using Eqn. 5 in Appendix, and the resulting values of parameters are shown in Table I.

(see Table I and Appendix, Eqn. 5). In addition, a non-competitive inhibitory effect of Ca^{2+} (K_I = 375 μM) was assumed in order to account for the decrease of ATPase activity at high Ca^{2+} concentrations (Fig. 4). A more complex model for the Ca^{2+} inhibition can be developed, for instance by considering the suggested inhibitory effect of the $CaATP^{2-}$ complex on the ATP site [37] but for the present purpose the used model was satisfactory. In our model, identical values of K_I were used for both the A and the B state. However, the activities of the A-state ATPase in Fig. 4 could be fitted equally well by using a higher value of K_I combined with a lower value of V, cf. Schatzmann's discussion [17] of this topic.

The determination of Ca^{2+} activation of the ATPase at low Ca^{2+} concentrations ($\leqslant 10^{-6}$ M) requires the presence of EGTA or a similar chelator of Ca^{2+}. It has been reported that EGTA influences the Ca^{2+} activation of the ATPase [38,39]. However, we found only small effects on Ca^{2+} activation of EGTA in concentrations ranging from 0.3 to 3 mM (unpublished data, cf. also Ref. 40). We therefore used the curves shown in Fig. 4 as estimates of the Ca^{2+} sensitivities of the proposed two states of the Ca^{2+} pump, and the

TABLE I

PARAMETERS OF MODEL FOR Ca^{2+}-PUMP ATPase

The parameter values were obtained by fitting Eqn. 5 in the Appendix to the experimental points in Fig. 4, using the method of least squares. The units are: c_i values (μM^{-1}), K_I (μM) and V (μmol/min per g protein). The values of V used for calculation of Ca^{2+} pump fluxes (V_p) were 308 (A-state) and 490 (B-state) μmol/min per l cells, provided a pump stoichiometry (see text) equal to one.

Parameter	A-state	B-state
c_1	0.15	1.5
c_2	0.001	1.5
c_3	0.08	0.4
c_4	0.001	0.05
K_I	375	375
V	44	70

Ca^{2+}-pump fluxes were calculated from the values given in Table I, assuming a pump stoichiometry n (i.e., mol transported Ca^{2+} per mol hydrolysed ATP) equal to 1 (the V values should be multiplied by 2 for $n = 2$).

Ca^{2+}-dependence of calmodulin binding

At low Ca^{2+} concentrations, calmodulin binds slowly to the Ca^{2+}-ATPase, resulting in a delay in the Ca^{2+} activation of the ATPase, and at high Ca^{2+} concentrations calmodulin dissociates slowly from the ATPase-calmodulin complex [21]. Fig. 5 shows the Ca^{2+} dependence of the overall rate constants for association (k_1) and dissociation (k_2) of the Ca^{2+}-calmodulin complex (Ca_iZ) and enzyme (E), illustrated by the overall reaction:

$$Ca_iZ + E_A \underset{k_2}{\overset{k_1}{\rightleftarrows}} E_B(Ca_iZ)$$

Values of k_1 and k_2 were determined previously [21] by measuring the rate of activation or deactivation of the ATPase at various concentrations of calmodulin and free Ca^{2+}. The experimental values of k_1 and k_2 from Ref. 21 were here fitted by a mathematical model (see Fig. 5, Table II and Appendix, Eqns. 6 and 7). Experimental values of k_1 could not be determined at the lowest Ca^{2+} concentrations due to the low activity of the Ca^{2+}-ATPase below 0.5 μM free Ca^{2+} (see Fig. 4).

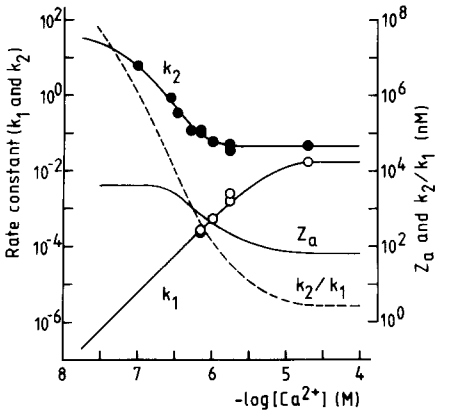

Fig. 5. Overall rate constants (k_1 and k_2) for calmodulin binding to Ca^{2+}-ATPase and hypothetical concentration of available calmodulin (Z_a), in dependence of the concentration of free Ca^{2+}. k_1 ($nM^{-1} \cdot min^{-1}$) and k_2 (min^{-1}) refer to association and dissociation, respectively, of the calmodulin-ATPase complex. The solid curves were fitted to the experimental points by using Eqns. 6 and 7 in Appendix, and the resulting values of parameters are shown in Table II. Z_a was calculated from Eqn. 8 in the Appendix by using the values: $Y_t = Z_t = 4$ μmol/l and $K_y = 0.4 \cdot k_2/k_1$.

The rate constants k_1 and k_2 were determined in Ca^{2+}/EGTA buffers [21] but the delay in activation of the Ca^{2+}-ATPase was not influenced by EGTA. For instance, determinations of k_1 and k_2 in experiments at 13 and 28 μM free Ca^{2+} conducted in the absence of Ca^{2+} chelator or in the presence of nitrilotriacetic acid did not deviate from determinations in the presence of EGTA (not shown).

TABLE II

PARAMETERS OF MODEL FOR OVERALL RATE CONSTANTS (k_1 AND k_2) FOR BINDING OF CALMODULIN TO Ca^{2+} PUMP ATPase

The a_i values were taken from Crouch and Klee [48]. The other parameter values were obtained by fitting Eqns. 6 and 7 in the Appendix to the experimental points in Fig. 5, using the method of least squares (cf. also Fig. 10 in the Appendix).

i	a_i (μM^{-1})	b_i (μM^{-1})	k_{1i} ($\mu M^{-1} \cdot min^{-1}$)	k_{2i} (min^{-1})
0			0	50
1	0.19	19	≤ 0.03	3.0
2	0.21	21	15	0.045
3	0.04	4	28	0.045
4	0.026	2.6	13.5	0.045

The cellular concentration of free calmodulin, available for the Ca^{2+} pump, depends on the presence of other calmodulin-binding proteins in the red cells. According to Penniston et al. [41], the total concentration of calmodulin-binding sites in the red cell cytoplasm may be comparable to the concentration of calmodulin. Very little is known about the Ca^{2+} dependence of calmodulin-binding to these proteins. The binding of calmodulin to troponin I [42] and to cAMP phosphodiesterase [43] seem to occur more quickly than that to the Ca^{2+}-ATPase [21], and calmodulin binds to the phosphodiesterase with higher affinity (2.5-times) than to the Ca^{2+}-ATPase.

In order to calculate the activity of the Ca^{2+} pump in the cell, where the concentration of calmodulin may be limiting, we have for simplicity assumed the existence of one cellular protein, Y, that competes with the Ca^{2+} pump for calmodulin. Protein Y was assumed to bind calmodulin much faster and with higher affinity than the Ca^{2+} pump, the Ca^{2+}-dependent dissociation constant being $K_y = 0.4 \cdot k_2/k_1$ (see Fig. 5). We can now calculate concentrations of free calmodulin (Z_a) available for the Ca^{2+} pump, at different Y_t values (see Appendix, Eqn. 8). Z_a decreased with increasing Ca^{2+} concentration, as in the example shown in Fig. 5.

This estimate of the concentration of available calmodulin is, of course, a rough approximation. A complete description of the competition between different cellular proteins for calmodulin would require the solution of one differential equation (analogous to Eqn. 4 in the Appendix) for each of the calmodulin-binding proteins.

Simulation of calcium transients

A change of cellular calcium (Ca_i) with time, caused by an increased Ca^{2+} influx, can be simulated by the aid of the model for regulation of cellular calcium, described in the Appendix.

The observed calcium transients mediated by ionophore A23187 could be accounted for in terms of this model, including the previously demonstrated delay in the activation of the Ca^{2+}-ATPase, i.e., the slow shift from the A- to the B-state [21], whereas models without delay did not explain the calcium transients. This is illustrated in Fig. 6.

Curve *A/B* in Fig. 6 represents a cellular

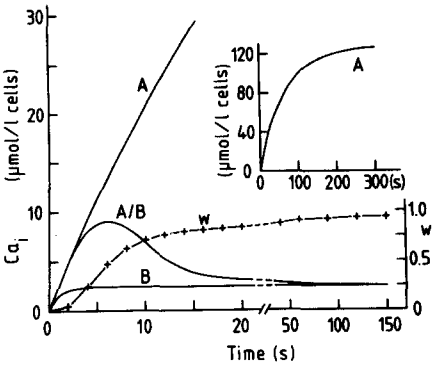

Fig. 6. Simulated changes of cellular calcium (Ca_i) and fraction of Ca^{2+} pumps in the B-state (w) calculated by a mathematical model. Curve *A/ B*, Ca_i when the Ca^{2+} pump is assumed to shift from the A to the B state, as indicated by curve w. Curve *A* (including insert), Ca_i when the Ca^{2+} pump remains in the A state, i.e., $w = 0$. Curve *B*, Ca_i when the Ca^{2+} pump shifts to the B-state without delay, i.e., $w = 1$. The curves represent solutions of Eqns. 2 and 4 in the Appendix, using calculated values of Ca^{2+} leak (Fig. 3), Ca^{2+} pump flux (Fig. 4 and Table I), overall rate constants (Fig. 5 and Table II), and the values: $Y_t = 0$, $Z_t = 4$ µmol/l and $E_t = 70$ nmol/l [29], ratio of ionized Ca^{2+} to total Ca in cells $\alpha = 0.3$, Ca^{2+}-pump stoichiometry $n = 1$. The simulated experimental conditions are those in Fig. 1, including addition of ionophore A23187 (8.8 µmol/l cells) at zero time to a suspension containing 20% cells and 100 µM $CaCl_2$. Ca^{2+} influx was calculated from curve 8.8 (Fig. 3) as y values, using the extracellular Ca^{2+} concentration, $Ca_0 = 100 - 0.25 \cdot Ca_i$. The A23187-mediated Ca^{2+} efflux was calculated from curve 8.8 as y/r^2 values (cf. Eqn. 1 in the Appendix), using the intracellular concentration of free Ca^{2+}, αCa_i.

calcium transient (Ca_i) obtained by solving the two differential equations (Eqns. 2 and 4) shown in the Appendix. Simultaneously, we obtained solutions for w (Fig. 6, curve w), referring to the fraction of B state, which increased with time and finally reached a steady state level, concurrently with the adjustment of Ca_i to a low steady-state level (curve *A/B*).

If the shift of Ca^{2+} pump from the A- to the B-state was assumed to occur without a delay, the calculations showed that Ca_i would rise to the low steady-state level within a few seconds and no initial Ca_i peak would occur (Fig. 6, curve *B*). If the Ca^{2+} pump was assumed to remain in the A-state, the calculated Ca_i would rise to a high level within 3–5 min and, again, no initial Ca_i peak would occur (Fig. 6, curve *A*).

In the calculations of the Ca^{2+} leak, L, we have assumed a membrane potential $E = -10$ mV and, correspondingly, a potential factor $r^2 = 2.1$ (see Eqn. 1 in the Appendix). The calculated calcium transients were not influenced by the choice of another r^2 value between 1 and 4.

The height and the duration of the calculated calcium transients depended on (1) the Ca^{2+} pump flux, V_p, and thereby the pump stoichiometry (see Table I), (2) the Ca^{2+} leak, L, (3) the ratio, α, of ionized calcium to total calcium inside the cell, (4) the concentration, Z_a, of available calmodulin. An increase in V_p, e.g., by the change of pump stoichiometry from 1 to 2, decreased the height and duration of the calcium transients, whereas an increase in L, a decrease of α, or a reduction of Z_a all resulted in increased height and duration of the calcium transients.

Decreasing concentrations, Z_a, of available calmodulin were introduced in the calculations by choosing increasing concentrations, Y_t, of the hypothetical calmodulin-binding protein Y, and Fig. 7 shows that these calculations resulted in calcium transients with increasing height and duration. As the Y_t value approached the total concentration, Z_t, of calmodulin (4 µmol/l) the relative effect of a change in Y_t increased. It appears that at all the chosen values of Y_t (Fig. 7) Ca_i was adjusted to low steady-state levels during the next 10–20 min. Changes in the calcium tran-

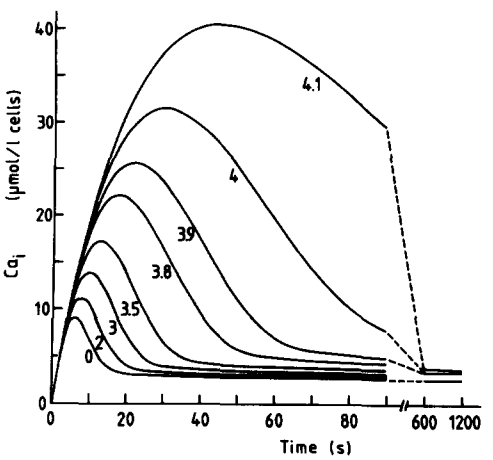

Fig. 7. Simulated calcium transients (Ca_i) at limiting concentrations of calmodulin. The curves are calculated as curve *A/B* in Fig. 6, using different Y_t values (µmol/l, as indicated on the curves). Increasing Y_t values imply reductions of free calmodulin (Z_a), available for the Ca^{2+} pump.

sients, as those in Fig. 7, could not be obtained, for instance, by using lower V values for the Ca^{2+} pump.

A simulated experiment with successive additions of ionophore A23187 to the cell suspension (Fig. 8) showed that the three A23187 additions resulted in increases of the fraction of B-state (w) and the occurrence of peak values of Ca_i, similar to those shown in Fig. 2. The fourth A23187 addition, however, had only a small influence on w (now equal to approx. 0.75) and no Ca_i peak occurred (cf. Fig. 2). Apparently, as the saturation with calmodulin is approached, the Ca^{2+} pump cannot be activated further by shift from the A to the B-state. This stage would have occurred at w values closer to 1 in case of lower Y_t values (less than 4 μmol/l).

Each of the A23187 additions shown in Fig. 8 increased the Ca^{2+} leak, L, 2- or 3-times, due to the increased Ca^{2+} influx. Shortly after the fourth A23187 addition, a peak value of L appeared, as a result of the great increase of Ca_i, leading to an increase in the A23187-induced Ca^{2+} efflux and a decrease in L (see Eqn. 1 in Appendix). Each of the first three A23187 additions resulted in an increase of the Ca^{2+}-pump flux, V_p, to a maximum value which exceeded the L value (Fig. 8, insert), then V_p decreased again, approaching the L value, and finally both values were adjusted to the steady-state values, in accordance with the experiment (Fig. 2).

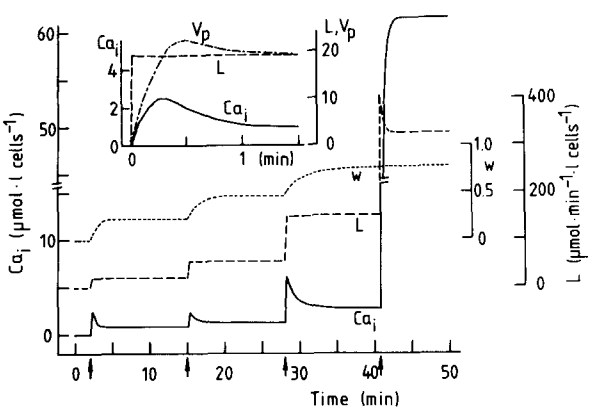

Fig. 8. Simulated changes of cellular calcium (Ca_i), the fraction of Ca^{2+} pumps in the B-state (w) and Ca^{2+} leak (L), calculated by assuming successive additions of ionophore A23187. Simulated experimental conditions are those in Fig. 2. The total A23187 concentration ([A]) after each addition (marked by arrows) was from left: 2.2, 4.4, 8.8, and 17.6 μmol/l cells. The curves are calculated as curve A/B in Fig. 6, using $Y_t = 4$ μmol/l and $\alpha = 0.4$. The A23187-mediated Ca^{2+} influx was calculated from curve 8.8 (Fig. 3) as $y \cdot ([A]/8.8)^{1.5}$ (cf. Results and Discussion), and Ca^{2+} efflux was calculated analogously (see Fig. 6). Insert: simulated changes of Ca_i, L, and Ca^{2+} pump flux (V_p) induced by addition of A23187 (2.2 μmol/l cells), here added at zero time.

The simulated experiments (Figs. 6 and 8) show that with a permanently high Ca^{2+} leak, maintained due to the presence of ionophore A23187, the fraction of pumps in the B-state remained high. This is in agreement with the fact that in the experiment in Fig. 2 no calcium transient occurred in response to the fourth A23187 addition.

In vivo, increases of cellular Ca^{2+} permeability are expected to be transient. The effect of a transient increase of the low native Ca^{2+} leak of human red cells is shown in Fig. 9. Recently, Lew et al. [44] determined the Ca^{2+} leak in human red cells suspended in plasma. The Ca^{2+} leak was 0.75 μmol/min per l cells, and using this value, we calculated that the fraction of pumps in the B-state (w) was below 0.1% and the physiological level of ionized calcium was approx. $6 \cdot 10^{-8}$ M, which is slightly higher than the values of 10^{-8} to $3 \cdot 10^{-8}$ M found by Lew et al. [44]. The calculated effects of the transient increase of Ca^{2+} influx (Fig. 9) were transient increases in Ca_i and pump

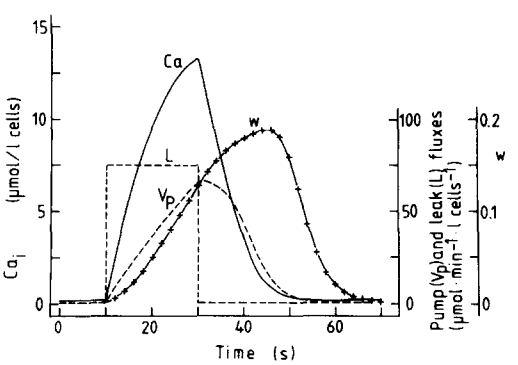

Fig. 9. Simulated transients of Ca_i, B-state fraction (w) and flux (V_p) of the Ca^{2+} pump, calculated by assuming a transient increase of Ca^{2+} leak (L). L was assumed to increase from 0.75 to 75 μmol/min per l cells during 20 s. The curves are calculated as curve A/B in Fig. 6, using $Y_t = 4$ μmol/l and $\alpha = 0.3$. The calculated steady-state values before the increase of L were: $Ca_i = 0.2$ μmol/l cells, $V_p = 0.75$ μmol/min per l cells and $w = 8 \cdot 10^{-4}$.

flux, V_p, and, further, an increase of the fraction of pumps in the B-state up to about 20%. It should be noticed that the value of w did not return to 0.1% until Ca_i had been reduced to the low physiological level for approx. 15 s.

Repeated transient increases in Ca^{2+} influx in red cells at a fixed quantity of ionophore A23187 were apparently obtained by Vestergaard-Bogind and Bennekou [24]. In their experiments, the pH of the unbuffered extracellular medium oscillated concurrently with an oscillating membrane potential due to opening and closing of the Ca^{2+}-sensitive K^+ channels. The competition between H^+ and Ca^{2+} for the ionophore induced changes in Ca^{2+} influx, leading to oscillating values of Ca_i [45]. Our hysteretic model can also account for such oscillations, but more quantiative data are needed to allow a closer analysis of this phenomenon.

In conclusion, our model supports the notion of a delay in the activation of the Ca^{2+} pump in human red cells. Previously, we have shown [20,21] that the Ca^{2+}-ATPase from red cells exhibits slow activation and deactivation in dependence of Ca^{2+} and calmodulin, similar to the hysteretic enzymes defined by Frieden [46]. In the present study it is shown that the occurrence of A23187-induced calcium transients (Fig. 1 and 2) can be explained by using a model that includes a delay in the activation of the Ca^{2+} pump, whereas a model without delay does not explain the experiments. Possibly, these hysteretic features also characterize Ca^{2+} pumps in other types of cell.

In addition, the simulations have demonstrated (see Fig. 7) that the size and duration of the calcium transients depends strongly on the cellular concentration of available calmodulin. Therefore, the proportions of competition for calmodulin between the Ca^{2+} pump and the several other calmodulin-binding proteins in cells should be examined.

Appendix

Model: cellular calcium concentration dependent on time

The intracellular calcium concentration (Ca_i) in red cells is determined by (1) the passive Ca^{2+} transport (Ca^{2+} leak, L) across the plasma membrane and (2) the active Ca^{2+} transport (V_p) energized by ATP via the Ca^{2+} pump located in the plasma membrane.

The Ca^{2+} leak can be expressed as the net flux (influx minus efflux) shown in Eqn. 1 (cf. Refs. 22, 30):

$$L = P(r^2[Ca^{2+}]_o - [Ca^{2+}]_i) \quad (1)$$

referring to permeability constant, P, and potential factor $r^2 = \exp(-2EF/RT)$, where E is the membrane potential, F and R the Faraday and gas constants and T absolute temperature. i and o refer to intracellular and extracellular compartments and $[Ca^{2+}]_i$ is equal to αCa_i, where α is the ratio of free Ca^{2+} to total Ca inside the cell, varying from 0.3–0.5 [22,33].

At pump-leak steady state, i.e., $L = V_p$, a constant value of Ca_i is attained, whereas at non-steady-state conditions, when L differs from V_p, Ca_i changes with time as shown in Eqn. 2:

$$dCa_i/dt = L - V_p \quad (2)$$

As a special case (see Eqn. 1), the final distribution of calcium at the electrochemical equilibrium ($L = 0$) will be $[Ca^{2+}]_i = r^2[Ca^{2+}]_0$ in depleted cells ($V_p = 0$).

The Ca^{2+} pump flux, V_p, is dependent on the activities of the supposed A-state (v_A) and B-state (v_B), corresponding to calmodulin-deficient and calmodulin-saturated pump state, respectively, as shown in Eqn. 3:

$$V_p = (1-w)v_A + wv_B \quad (3)$$

where w, the fraction of B state, depends on the concentration of free Ca^{2+}. In addition, w is time-dependent [21]:

$$dw/dt = k_1(1-w)(Z_a - wE_t) - k_2w \quad (4)$$

where k_1 and k_2 are rate constants for association and disociation, respectively, of calmodulin to the pump enzyme. Z_a is the concentration of free calmodulin, available for the pump enzyme, and E_t is the total concentration of pump enzyme.

The two differential equations (Eqns. 2 and 4) can now be solved by using a numerical method, and the solutions provide us with data for Ca_i and w as functions of time (see Calculations below).

Ca^{2+} pump activities, v_A and v_B, dependent on Ca^{2+}

v_A and v_B are calculated by means of a Ca^{2+}-ATPase model (Eqn. 5) with four calcium-binding sites [31] and including a non-competitive inhibitory effect of Ca^{2+} at high concentrations (K_I = 375 μM):

$$v = \frac{V}{4(1 + X/K_I)}\left[\sum_{i=1}^{i=4} iK_iX^i \Big/ \left(1 + \sum_{i=1}^{i=4} K_iX^i\right)\right] \quad (5)$$

where $X = [Ca^{2+}]_i$, V is the maximum velocity at the chosen conditions, $K_i = c_1c_2 \ldots c_i$, where c_1, c_2 and c_i are the macroscopic binding constants for the first, second and ith calcium ion that binds to the enzyme.

The calculated values of V, K_I and c_i, based on the experimental values from Fig. 4, are given in Table I.

Rate constants, k_1 and k_2, dependent on Ca^{2+}

The time-dependent shift between the A state and the B state of the pump enzyme is supposed to follow the kinetic scheme in Fig. 10, showing that the binding of different calcium-calmodulin complexes (Ca_iZ) converts the enzyme to the activated B state ($E_B(Ca_iZ)$).

The overall rate constants for association (k_1) and dissociation (k_2) depend on the partial rate constants (k_{1i} and k_{2i}, see Fig. 10) as described in Eqns. 6 and 7:

$$k_1 = \sum_{i=0}^{i=4} k_{1i}C_iX^i \Big/ \sum_{i=0}^{i=4} C_iX^i \quad (6)$$

$$k_2 = \sum_{i=0}^{i=4} k_{2i}Q_iX^i \Big/ \sum_{i=0}^{i=4} Q_iX^i \quad (7)$$

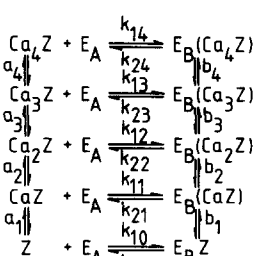

Fig. 10. Kinetic model for binding of Ca^{2+}-calmodulin complexes (Ca_iZ) to Ca^{2+}-pump ATPase (E).

since $[Ca_iZ] = C_i[Z]X^i$ and $[E_B(Ca_iZ)] = Q_i[E_BZ]X^i$, where $X = [Ca^{2+}]_i$, $C_i = a_1a_2 \ldots a_i$ and $Q_i = b_1b_2 \ldots b_i$ ($C_0 = Q_0 = 1$), a_i and b_i being the macroscopic binding constants for calcium binding to the ith site of calmodulin that is free of enzyme (a_i) or associated with enzyme (b_i).

The values of k_{1i}, k_{2i}, a_i and b_i, calculated partly on the basis of the experimental values from Fig. 5, are given in Table II.

Available calmodulin, Z_a, dependent on Ca^{2+}

If Z_t and Y_t refer to the total cellular concentrations of calmodulin and a hypothetical calmodulin-binding protein, Y, and YZ refers to the complex of Y and calmodulin, then the dissociation constant is

$$K_y = (Y_t - [YZ])(Z_t - [YZ])/[YZ]$$

from which a quadratic equation can be derived:

$$[YZ]^2 - (Y_t + Z_t + K_y)[YZ] + Y_tZ_t = 0$$

The concentration of free calmodulin, $Z_a = Z_t - [YZ]$, available for the Ca^{2+} pump, is then calculated from Eqn. 8:

$$Z_a = Z_t - \left(Y_t + Z_t + K_y - \sqrt{\left((Y_t + Z_t + K_y)^2 - 4Y_tZ_t\right)}\right)/2 \quad (8)$$

In the calculations we put $K_y = 0.4 \cdot k_2/k_1$ (cf. Eqns. 6 and 7) and, therefore, Z_a depends on the Ca^{2+} concentration, i.e., Z_a decreases with increasing Ca^{2+} (see Fig. 5).

Calculations

The calculations were done on a desk computer (Sharp PC-1500), programmed in BASIC language. We used a programme (modified from Sharp Manual) for the solution of two simultaneous differential equations of first order (Eqns. 2 and 4 above), based on the Runge-Kutta-Gill method (cf. Ref. 47). The method is iterative. The calculations were carried out by using the initial values $Ca_i = 0$ and $w = 0$ at zero time, the time values were increased stepwise, and for each step corresponding values of Ca_i, w, and all the parameters

(L, V_p, v_A, v_B, k_1, k_2 and Z_a) were calculated from the equations above.

Acknowlegements

We wish to thank Dr. Bent Vestergaard-Bogind for helpful discussions and Hanne Jepsen for valuable technical assistance. This work was supported by Danish Natural Science Research Council and by The International Union of Biochemistry.

References

1 Tsien, R.Y., Pozzan, T. and Rink, T.J. (1982) Nature 295, 68–71
2 Rink, T.J., Smith, S.W. and Tsien, R.Y. (1982) J. Physiol. 324, 53P-54P
3 Ashley, C.C. (1982) Biochem. Soc. Trans. 10, 212
4 Kovács, L., Ríos, E. and Schneider, M.F. (1979) Nature 279, 391–396
5 Eusebi, F., Miledi, R. and Takahashi, T. (1980) Nature 284, 560–561
6 Palade, P. and Vergara, J. (1982) J. Gen. Physiol. 79, 679–707
7 Fabiato, A. (1981) J. Gen. Physiol. 78, 457–497
8 Gorman, A.L.F., Hermann, A. and Thomas, M.V. (1981) Fed. Proc. 40, 2233–2239
9 Williams, J.A. (1980) Am. J. Physiol. 238, G269–G279
10 Baker, P.F. and Knight, D.E. (1981) Phil. Trans. R. Soc. Lond. B 296, 83–103
11 Wollheim, C.B. and Sharp, G.W.G. (1981) Physiol. Rev. 61, 914–969
12 Cuthbertson, K.S.R., Whittingham, D.G. and Cobbold, P.H. (1981) Nature 294, 754–757
13 Lehninger, A.L., Fiskum, G., Vercesi, A. and Tew, W. (1981) in Calcium and Phosphate Transport Across Biomembranes (Bronner, F. and Peterlik, M., eds.), pp. 73–78, Academic Press, New York
14 Blaustein, M.P. and Rasgado-Flores, H. (1981) in Calcium and Phosphate Transport Across Biomembranes (Bronner, F. and Peterlik, M., eds.), pp. 53–58, Academic Press, New York
15 Hagiwara, S. (1981) in The Mechanism of Gated Calcium Transport Across Biological Membranes (Ohnishi, S.T. and Endo, M., eds.), pp. 3–7, Academic Press, New York
16 Carafoli, E. (1981) in Calcium and Phosphate Transport Across Biomembranes (Bronner, F. and Peterlik, M., eds.), pp. 9–14, Academic Press, New York
17 Schatzman, H.J. (1982) in Membrane Transport of Calcium (Carafoli, E., ed.), pp. 41–108, Academic Press, New York
18 Roufogalis, B.D. (1979) Can. J. Physiol. Pharmacol. 57, 1331–1349
19 Sarkadi, B. (1980) Biochim. Biophys. Acta 604, 159–190
20 Scharff, O. (1981) Cell Calcium 2, 1–27
21 Scharff, O. and Foder, B. (1982) Biochim. Biophys. Acta 691, 133–143
22 Ferreira, H.G. and Lew, V.L. (1976) Nature 259, 47–49
23 Lew, V.L. and Ferreira, H.G. (1978) in Current Topics in Membranes and Transport (Bronner, F. and Kleinzeller, A., eds.), Vol. 10, pp. 217–277, Academic Press, New York
24 Vestergaard-Bogind, B. and Bennekou, P. (1982) Biochim. Biophys. Acta 688, 37–44
25 Szász, I., Sarkadi, B. and Gárdos, G. (1977) J. Membrane Biol. 35, 75–93
26 Larsen, F.L., Katz, S. and Roufogalis, B.D. (1981) Nature 294, 667–668
27 Cameron, B.F. and Smariga, P.E. (1981) Acta Biol. Med. Germ. 40, 771–777
28 Varecka, L. and Carafoli, E. (1982) J. Biol. Chem. 257, 7414–7421
29 Foder, B. and Scharff, O. (1981) Biochim. Biophys. Acta 649, 367–376
30 Lew, V.L. and Brown, A.M. (1979) in Detection and Measurement of Free Ca^{2+} in Cells (Ashley, C.C. and Campbell, A.K., eds.), pp. 423–432, Elsevier, Amsterdam
31 Scharff, O. (1976) Biochim. Biophys. Acta 443, 206–218
32 Scharff, O. (1979) Anal. Chim. Acta 109, 291–305
33 Scharff, O., Foder, B. and Skibsted, U. (1983) Acta Physiol. Lat. Am., in the press
34 Lew, V.L., and Simonsen, L.O. (1980) J. Physiol. 308, 60P
35 Valeri, C.R. (1974) in The Red Blood Cell (Surgenor, D.M., ed.), Vol. 1, pp. 511–574, Academic Press, New York
36 Flatman, P. and Lew, V.L. (1977) Nature 267, 360–362
37 Muallem, S. and Karlish, S.J.D. (1981) Biochim. Biophys. Acta 647, 73–86
38 Sarkadi, B., Schubert, A. and Gárdos, G. (1979) Experientia 35, 1045–1047
39 Al-Jobore, A. and Roufogalis, B.D. (1981) Biochim. Biophys. Acta 645, 1–9
40 Waisman, D.M., Gimble, J.M., Goodman, D.B.P. and Rasmussen, H. (1981) J. Biol. Chem. 256, 409–414
41 Penniston, J.T., Graf, E. and Itano, T. (1980) Ann. N. Y. Acad. Sci. 356, 245–256
42 Schimerlik, M.I., Malencik, D.A., Anderson, S.R. and Shalitin, Y. (1982) Biochem. Biophys. Res. Commun. 106, 1331–1339
43 Wang, J.H., Sharma, R.K., Huang, C.Y., Chau, V. and Chock, P.B. (1980) Ann. N. Y. Acad. Sci. 356, 190–204
44 Lew, V.L., Tsien, R.Y., Miner, C. and Bookchin, R.M. (1982) Nature 298, 478–481
45 Vestergaard-Bogind, B. (1983) Biochim. Biophys. Acta 730, 285–294
46 Frieden, C. (1979) Annu. Rev. Biochem. 48, 471–489
47 Ames, W.F. (1968) Nonlinear Ordinary Differential Equations in Transport Processes, Mathematics in Science and Engineering Vol. 42, pp. 218–224, Academic Press, New York
48 Crouch, T.H. and Klee, C.B. (1980) Biochemistry 19, 3692–3698